Computational Modeling of Temperature-Dependent Wavefields in Fluid-Saturated Porous Media

Evgeniy Romenski[1(✉)] and Galina Reshetova[2]

[1] Sobolev Institute of Mathematics SB RAS, Novosibirsk 630090, Russia
evrom@math.nsc.ru
[2] Institute of Computational Mathematics and Mathematical Geophysics SB RAS, Novosibirsk 630090, Russia
kgv@nmsf.sscc.ru

Abstract. A computational model is presented for simulations small amplitude wavefields in a deformable porous medium saturated with a compressible fluid under temperature variations. The model is based on the governing equations derived with the use of the theory of Symmetric Hyperbolic Thermodynamically Compatible (SHTC) systems in conjunction with the efficient staggered grid finite difference numerical method. It is numerically shown that the characteristics of wavefields in a saturated porous medium strongly depend on the porosity, which varies with temperature.

Keywords: Wavefield simulation · Fluid saturated porous medium · Staggered Grid Finite Difference Scheme

1 Introduction

Modeling of wave processes in porous media is of interest for many practical problems of applied geophysics. This area of research is becoming especially relevant in connection with the development of digital technologies for twins of geological objects.

In this paper, we use the Symmetric Hyperbolic Thermodynamically Compatible (SHTC) model to study small amplitude waves in a layered medium containing a porous layer for temperature-varying porosity. The purpose of the study is to reveal the features of the behavior of reflected waves from a porous layer, saturating liquid in which undergoes a phase transition from a solid to a

The mathematical model was developed by E. Romenski within the framework of the state contract of the Sobolev Institute of Mathematics (project no. FWNF-2022-0008). Numerical method was developed by G. Reshetova and supported by the Russian Science Foundation grant no. 22-21-00759. E. Romenski's contribution to numerical modeling was supported by the Russian Science Foundation grant no. 22-11-00104.

© The Author(s), under exclusive license to Springer Nature Switzerland AG 2023
O. Gervasi et al. (Eds.): ICCSA 2023 Workshops, LNCS 14106, pp. 103–115, 2023.
https://doi.org/10.1007/978-3-031-37111-0_8

liquid state (in this case, porosity increases). Such features will help, for example, outline approaches to the development of geophysical methods for searching for and monitoring the development of natural accumulations of gas hydrates.

As a basis for such consideration, we choose the thermodynamically compatible model developed in [1–4]. This choice is due to the flexibility of the model, which allows generalizations to the case of a multiphase saturating liquid and finite deformations of the skeleton, the possibility of taking into account phase transformations, and so on. The use of the generally accepted Biot approach for modeling porous media [5–7] is problematic, due to the difficulties that arise when trying to generalize Biot's model to describe the phenomena mentioned above. The theory of SHTC systems of conservation laws [8–10], applied to the modeling of multiphase media, makes it possible to design a mathematically well-posed hyperbolic model for the flow of a multiphase compressible mixture in a deformable porous skeleton, which satisfies the laws of nonequilibrium thermodynamics [1–4]. Note that in the case of small deformations, the SHTC model of a porous medium saturated with a compressible liquid qualitatively gives the same results in describing wavefields as the Biot's model [1].

The rest of the paper is organized as follows. Section 2 formulates the general equations of the SHTC model of a porous medium in the case of finite deformations and its linearized version for the case of small deformations. Section 3 presents a brief description of the finite difference scheme on a staggered grid, and Sect. 4 presents a numerical test problem that demonstrates the features of wave propagation in a layered medium for different porosities, which can vary depending on temperature.

2 Symmetric Hyperbolic Thermodynamically Compatible System of Deformed Saturated Porous Medium

2.1 A General Master System for Processes in a Deformed Saturated Porous Medium

Consider a deformable porous medium saturated with the compressible fluid. We restrict ourselves to single entropy approximation [1], which is admissible for small variations in the phase temperatures. The governing PDEs of the general SHTC model in the case of finite strains and in the single entropy approximation are read as

$$\frac{\partial \rho v^i}{\partial t} + \frac{\partial (\rho v^i v^k + \rho^2 E_\rho \delta_{ik} + w^i E_{w^k} + \rho A_{ki} E_{A_{kj}})}{\partial x_k} = 0, \tag{1}$$

$$\frac{\partial A_{ik}}{\partial t} + \frac{\partial A_{im} v^m}{\partial x_k} + v^j \left(\frac{\partial A_{ik}}{\partial x_j} - \frac{\partial A_{ij}}{\partial x_k} \right) = -\frac{\psi_{ik}}{\theta}, \tag{2}$$

$$\frac{\partial \rho}{\partial t} + \frac{\partial \rho v^k}{\partial x_k} = 0, \tag{3}$$

$$\frac{\partial \rho c_1}{\partial t} + \frac{\partial (\rho c_1 v^k + \rho E_{w^k})}{\partial x_k} = 0, \tag{4}$$

$$\frac{\partial w^k}{\partial t} + \frac{\partial (w^l v^l + E_{c_1})}{\partial x_k} + v^l \left(\frac{\partial w^k}{\partial x_l} - \frac{\partial w^l}{\partial x_k} \right) = -\frac{\lambda_k}{\theta_2}, \tag{5}$$

$$\frac{\partial \rho \alpha_1}{\partial t} + \frac{\partial \rho \alpha_1 v^k}{\partial x_k} = -\frac{\rho \varphi}{\theta_1}, \tag{6}$$

$$\frac{\partial \rho s}{\partial t} + \frac{\partial \rho s v^k}{\partial x_k} = \frac{\rho}{\theta E_s} \psi_{ik} \psi_{ik} + \frac{\rho}{\theta_1 E_s} \varphi^2 + \frac{\rho}{\theta_2 E_s} \lambda_k \lambda_k \geq 0. \tag{7}$$

Here (1) is the momentum conservation law for the entire porous medium, (2) is the evolution equation for the distortion (elastic deformation gradient), (3) is the mass conservation law for the entire medium, (4) is the mass conservation law for the saturating fluid, (5) is the equation for the relative velocity, (6) is the balance equation for the fluid volume fraction and (7) is the entropy balance law. The following state variables are used: α_1 is the volume fraction of saturating fluid ($\alpha_2 = 1 - \alpha_1$ - volume fraction of deformable skeleton), ρ_1, ρ_2 are the mass densities of the fluid and the skeleton, respectively, $\rho = \alpha_1 \rho_1 + \alpha_2 \rho_2$ is the mass density of the mixture, $c_1 = \alpha_1 \rho_1 / \rho$ is the mass fraction of the fluid ($c_2 = 1 - c_1$ - the mass fraction of the skeleton), $v^k = c_1 v_1^k + c_2 v_2^k$ is the mixture velocity, v_1^k, v_2^k are velocities of fluid and skeleton, respectively, $w_k = v_1^k - v_2^k$ is the relative velocity and s is the entropy of the mixture.

The main closing relation for system (1)–(7) is the generalized internal energy E which we take in the form

$$E = E_1(c_1, |\mathbf{w}|) + E_2(\alpha_1, c_1, \rho, s) + E_3(c_1, \rho, s, A_{ik}). \tag{8}$$

The kinetic energy of the relative motion E_1 is defined as

$$E_1(c_1, |\mathbf{w}|) = \frac{1}{2} c_1 (1 - c_1) \rho w^j w^j. \tag{9}$$

The energy of volumetric deformation E_2 is defined as

$$E_2(\alpha_1, c_1, \rho, s) = c_1 e_1(\rho_1, s) + c_2 e_2(\rho_2, s) = c_1 e_1 \left(\frac{\rho c_1}{\alpha_1}, s \right) + c_2 e_2 \left(\frac{\rho c_2}{\alpha_2}, s \right). \tag{10}$$

The shear energy E_3 depends on the distortion of the entire solid-fluid mixture element and is read as

$$E_3 = \frac{1}{8} c_2 c_s^2 \left(tr(\mathbf{g}^2) - 3 \right), \tag{11}$$

where c_s is the shear velocity of sound of the solid skeleton, and $\mathbf{g}$ is the normalized Finger strain tensor: $\mathbf{g} = \mathbf{G}(det\ \mathbf{G})^{-1/3}$, $\mathbf{G} = \mathbf{A}^T\mathbf{A}$.

There are three dissipative source terms in the above system corresponding to shear stress relaxation (Eq. (2)), relative velocity relaxation (Eq. (5)), and phase pressure relaxation to a common value (Eq. (6)). There is a source term in the entropy Eq. (7), which describes the growth of entropy due to described above relaxation processes. The dissipative source terms are proportional to thermodynamic forces:

$$\psi_{ik} = E_{A_{ik}}, \quad \lambda_k = E_{w_k}, \quad \phi = E_\alpha,$$

and parameters $\theta, \theta_1, \theta_2$ characterize the rate of relaxation and can be a functions of state variables.

Using the chosen internal energy, the thermodynamic forces can be calculated as

$$E_{\alpha_1} = \frac{p_2 - p_1}{\rho}, \quad p = \rho^2 E_\rho = \alpha_1 p_1 + \alpha_2 p_2, \quad p_i = \rho_i^2 \frac{\partial e_i}{\partial \rho_i}, \ (i = 1, 2) \tag{12}$$

$$\frac{\partial E}{\partial \mathbf{A}} = \frac{c_s^2}{2}\mathbf{A}^{-T}\left(\mathbf{g}^2 - \frac{tr(\mathbf{g}^2)}{3}\delta_{ij}\right), \quad \sigma_{ij} = -\frac{\rho c_s^2}{2}\left(g_{ik}g_{kj} - \frac{1}{3}g_{lk}g_{kl}\delta_{ij}\right), \tag{13}$$

$$E_{c_1} = e_1 + \frac{p_1}{\rho_1} - e_2 - \frac{p_2}{\rho_2} + (1 - 2c_1)\frac{w^i w^i}{2} - c_s^2\left(tr(\mathbf{g}^2) - 3\right), \tag{14}$$

$$E_{w^i} = c_1 c_2 w^i, \quad E_s = T = c_1\frac{\partial e_1}{\partial s} + c_2\frac{\partial e_2}{\partial s}. \tag{15}$$

Equations (1)–(7) can be transformed to a symmetric hyperbolic system and satisfy the thermodynamic laws - energy conservation and entropy growth [1]. They can be used to simulate complex processes in a porous medium, including fluid flows in a deformable medium accompanied by temperature variations.

2.2 Linear System for Modeling the Propagation of Small Amplitude Waves

We are interested in modeling small amplitude wavefields, and for this purpose it is convenient to linearize (1)–(7) under the assumption of small deformations and small temperature variations. We also assume instantaneous pressure relaxation, which is natural to assume for a small pore space, since the phase pressures are equalized due to the propagation and reflection of sound waves in the pores. After linearization we come to the hyperbolic system of linear PDEs written in terms of velocities, relative velocities, pressure and shear stress:

$$\rho_0 \frac{\partial V^i}{\partial t} + \frac{\partial P}{\partial x_i} - \frac{\partial \Sigma_{ik}}{\partial x_k} = 0, \tag{16}$$

$$\frac{\partial W^k}{\partial t} + \left(\frac{1}{\rho_1^0} - \frac{1}{\rho_2^0}\right) \frac{\partial P}{\partial x_k} = -\frac{c_1^0 c_2^0}{\theta_2} W^k, \tag{17}$$

$$\frac{\partial P}{\partial t} + K \frac{\partial V^k}{\partial x_k} + \frac{\alpha_1^0 \alpha_2^0}{\rho_0} \left(\rho_2^0 - \rho_1^0\right) K \frac{\partial W^k}{\partial x_k} = F, \tag{18}$$

$$\frac{\partial \Sigma_{ik}}{\partial t} - \mu \left(\frac{\partial V^i}{\partial x_k} + \frac{\partial V^k}{\partial x_i} - \frac{2}{3}\delta_{ik} \frac{\partial V^j}{\partial x_j}\right) = -\frac{\Sigma_{ik}}{\tau}. \tag{19}$$

Here V^i, W^k, P, Σ_{ik} are, respectively, small perturbations of the velocity, relative velocity, pressure, and shear stress tensor of the steady unstressed state. $K = (\alpha_1^0 K_1^{-1} + \alpha_2^0 K_2^{-1})^{-1}$ is the bulk modulus of the mixture, $\mu = \alpha_2^0 \rho_2^0 c_s^2$ is the shear modulus of the mixture (it is assumed that the shear modulus in the fluid is equal to zero). $K_1 = \rho_1^0 \frac{\partial p_1}{\partial \rho_1}|_{\rho_1=\rho_1^0}$, $K_2 = \rho_2^0 \frac{\partial p_2}{\partial \rho_2}|_{\rho_2=\rho_2^0}$ are the bulk moduli of fluid and solid, respectively. The index 0 denotes the initial unperturbed values of the state variables in the stationary state.

Equations (17) and (19) contain dissipation mechanisms corresponding to interfacial friction and shear stress relaxation, respectively. The source term $F = F(x,t)$ presented in (18) is designed to generate waves in the medium.

We are interested in studying the properties of wavefields depending on temperature. Although in (16)–(19) the temperature is not explicitly represented, its influence can be seen from the change in the coefficients depending on the temperature. Of greatest interest is the change in the wave properties of the medium for the case of phase changes in the saturating liquid during its transformation from a solid to a liquid state. Examples of such phenomena are the thawing of permafrost and the decomposition of gas hydrates. Apparently, in this case, the temperature dependence of the coefficient of interfacial friction and initial porosity can have the highest influence on the properties of wave fields. Below we will numerically study only the effect of changing porosity on wavefields and see that this effect is significant.

3 Finite Difference Method

The numerical method that we use for simulations is based on the staggered grid finite difference scheme [11,12]. We consider the two-dimensional case and introduce new notations for the coordinates $x_1 = x$, $x_2 = y$ and the state variables $V_1, = V_x$, $V_2 = V_y$, $W_1 = W_x$, $W_2 = W_y$, $\Sigma_{11} = \Sigma_{xx}$, $\Sigma_{22} = \Sigma_{yy}$, $\Sigma_{12} = \Sigma_{xy}$. In the space and time domain (t,x,y) let us introduce a grid with the integer nodes $t^n = n\Delta t$, $x_i = i\Delta x$, $y_j = j\Delta y$ and the half-integer nodes $t^{n+1/2} = (n+1/2)\Delta t$, $x_{i+1/2} = (i+1/2)\Delta x$, $y_{j+1/2} = (j+1/2)\Delta y$, where Δt, Δx, and Δy denote grid intervals in time and space.

For a discrete function $f_{i,j}^n = f(t^n, x_i, y_j)$ let us define central difference operators

$$D_t[f]_{i,j}^n = \frac{(f)_{i,j}^{n+1/2} - (f)_{i,j}^{n-1/2}}{\Delta t}, \qquad A_t[f]_{i,j}^n = \frac{(f)_{i,j}^{n+1/2} + (f)_{i,j}^{n-1/2}}{2}, \tag{20}$$

and fourth-order central operators (Levander stencil)

$$D_x[f]^n_{i,j} = \frac{1}{\Delta x}\left\{\frac{9}{8}\left((f)^n_{i+1/2,j} - (f)^n_{i-1/2,j}\right) - \frac{1}{24}\left((f)^n_{i+3/2,j} - (f)^n_{i-3/2,j}\right)\right\}, \tag{21}$$

$$D_y[f]^n_{i,j} = \frac{1}{\Delta y}\left\{\frac{9}{8}\left((f)^n_{i,j+1/2} - (f)^n_{i,j-1/2}\right) - \frac{1}{24}\left((f)^n_{i,j+3/2} - (f)^n_{i,j-3/2}\right)\right\}. \tag{22}$$

Finite-difference scheme on a staggered grid is based on the finite-volume discretization method [13], which is used for systems of equations arising from physical conservation laws. To this end, we define medium parameters and wavefield components at different time-space grid nodes. In the method being used, we determine the state variables of the medium at different nodes of the space-time grid. It is assumed that the material parameters are constant within each grid cell $[x_{i-1/2}, x_{i+1/2}] \times [y_{j-1/2}, y_{j+1/2}]$ with possible discontinuities along the grid lines. The mixture velocities V_x, V_y and the relative velocities W_x, W_y are defined at points numbered $(i+1/2, j)$, $(i, j+1/2)$ as $(V_x)^n_{i+1/2,j}$, $(V_y)^n_{i,j+1/2}$, $(W_x)^n_{i+1/2,j}$, $(W_y)^n_{i,j+1/2}$. The pressure and the normal components of the deviatoric stress are defined at points (i,j) as $(P)^{n+1/2}_{i,j}$, $(\Sigma_{xx})^{n+1/2}_{i,j}$, $(\Sigma_{yy})^{n+1/2}_{i,j}$, and the shear stress is defined at points $(i+1/2, j+1/2)$ as $(\Sigma_{xy})^{n+1/2}_{i+1/2,j+1/2}$. The details can be seen on Fig. 1.

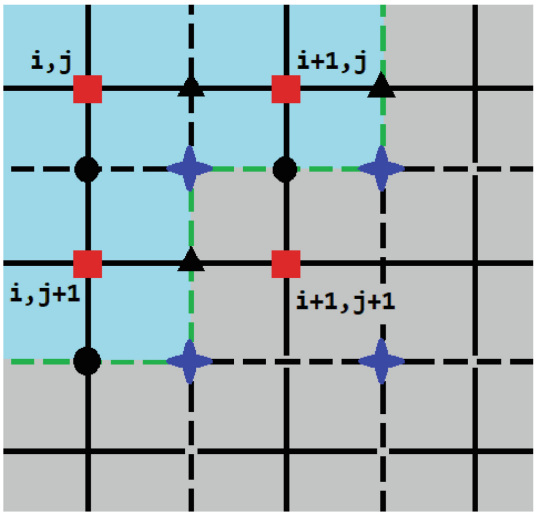

Fig. 1. The relative position of the wavefield components on the staggered grid near the medium interface: red square (integer i and j) - $\Sigma_{xx}, \Sigma_{yy}, P$; blue star (half-integer i and j) - Σ_{xy}; black triangle (half-integer i, integer j) - V_x, W_x; black circle (integer i, half-integer j) - V_y, W_y. The green dashed line is the interface on the staggered grid. (Color figure online)

The constructed finite difference scheme reads as

$$D_t[V_x]^{n-1/2}_{i+1/2,j} = -\left\langle 1/\rho^0 \right\rangle_{i+1/2,j} D_x[P]^{n-1/2}_{i+1/2,j} + \left\langle 1/\rho^0 \right\rangle_{i+1/2,j} \left(D_x[\Sigma_{xx}]^{n-1/2}_{i+1/2,j} + D_y[\Sigma_{xy}]^{n-1/2}_{i+1/2,j} \right), \tag{23}$$

$$D_t[V_y]^{n-1/2}_{i,j+1/2} = -\left\langle 1/\rho^0 \right\rangle_{i,j+1/2} D_y[P]^{n-1/2}_{i,j+1/2} + \left\langle 1/\rho^0 \right\rangle_{i,j+1/2} \left(D_x[\Sigma_{xy}]^{n-1/2}_{i,j+1/2} + D_y[\Sigma_{yy}]^{n-1/2}_{i,j+1/2} \right), \tag{24}$$

$$D_t[W_x]^{n-1/2}_{i+1/2,j} = -\left\langle 1/\rho_1^0 - 1/\rho_2^0 \right\rangle_{i+1/2,j} D_x[P]^{n-1/2}_{i+1/2,j} - \left\langle c_1^0 c_2^0/\theta_2 \right\rangle_{i+1/2,j} A_t[W_x]^{n-1/2}_{i+1/2,j}, \tag{25}$$

$$D_t[W_y]^{n-1/2}_{i,j+1/2} = -\left\langle 1/\rho_1^0 - 1/\rho_2^0 \right\rangle_{i,j+1/2} D_y[P]^{n-1/2}_{i,j+1/2} - \left\langle c_1^0 c_2^0/\theta_2 \right\rangle_{i,j+1/2} A_t[W_y]^{n-1/2}_{i,j+1/2}, \tag{26}$$

$$D_t[P]^n_{i,j} = -(K)_{i,j} \left(D_x[V_x]^n_{i,j} + D_y[V_y]^n_{i,j} \right) - \left((\rho_2^0 - \rho_1^0)\alpha_1^0 \alpha_2^0 K/\rho^0 \right)_{i,j} \left(D_x[W_x]^n_{i,j} + D_y[W_y]^n_{i,j} \right), \tag{27}$$

$$D_t[\Sigma_{xx}]^n_{i,j} = (\mu)_{i,j} \left(\frac{4}{3} D_x[V_x]^n_{i,j} - \frac{2}{3} D_y[V_y]^n_{i,j} \right) - (1/\tau)_{i,j} A_t[\Sigma_{xx}]^n_{i,j}, \tag{28}$$

$$D_t[\Sigma_{yy}]^n_{i,j} = (\mu)_{i,j} \left(\frac{4}{3} D_y[V_y]^n_{i,j} - \frac{2}{3} D_x[V_x]^n_{i,j} \right) - (1/\tau)_{i,j} A_t[\Sigma_{yy}]^n_{i,j}, \tag{29}$$

$$D_t[\Sigma_{xy}]^n_{i+1/2,j+1/2} = \{\mu\}_{i+1/2,j+1/2} \left(D_x[\Sigma_y]^n_{i+1/2,j+1/2} + D_y[V_x]^n_{i+1/2,j+1/2} \right) - \{1/\tau\}_{i+1/2,j+1/2} A_t[\Sigma_{xy}]^n_{i+1/2,j+1/2}, \tag{30}$$

where the parameters of the medium on the staggered grid are defined as volume arithmetic averaging

$$\langle f \rangle_{i+1/2,j} = (f_{i,j} + f_{i+1,j})/2, \qquad \langle f \rangle_{i,j+1/2} = (f_{i,j} + f_{i,j+1})/2, \tag{31}$$

or harmonic averaging [14]

$$f_{i+1/2,j+1/2} = \left[\frac{1}{4} \left(\frac{1}{f_{i,j}} + \frac{1}{f_{i+1,j}} + \frac{1}{f_{i,j+1}} + \frac{1}{f_{i+1,j+1}} \right) \right]^{-1}. \tag{32}$$

4 Numerical Test Problem

Let us consider a simple model of a medium consisting of a "gas hydrate" (a substance that changes from a solid to a liquid when the temperature rises) layer inside a homogeneous elastic medium. The choice of such a simplified model is due to the desire to reveal the main features of the behavior of reflected waves from a layer of gas hydrates. The presence of specific properties of wave behavior can help formulate prognostic signs of the existence of gas hydrates in the fields of seismic waves, as well as outline approaches to the development of geophysical

methods for searching and analyzing the evolutionary processes of gas hydrate deposits.

The velocities of seismic waves in a homogeneous medium were selected based on the plot of velocities characteristic of gas hydrates as a function of temperature [15] and are presented in Table 1.

Table 1. Material parameters of the media.

State	Parameter	Notation	Value	Unit
Surrounding medium	Longitudinal sound velocity	V_p	2400	m/s
	Shear sound velocity	V_s	1800	m/s
	Density	ρ_2	2500	kg/m^3
Gas hydrate *Solid state*	Longitudinal sound velocity	V_p	3800	m/s
	Shear sound velocity	V_s	2400	m/s
	Density	ρ_2	2500	kg/m^3
Gas hydrate *Liquid state*	Longitudinal sound velocity	V_p	1300	m/s
	Shear sound velocity	V_s	800	m/s
	Density	ρ_1	1040	kg/m^3
Dissipative parameters	Interphase friction	$c_1^0 c_2^0/\theta_2$	$3.36 \cdot 10^{-7}$	s^{-1}
	Relaxation time	τ	10^{-4}	s

Table 1 lists the parameters that make it possible to describe a layer of gas hydrates as a poroelastic medium consisting of a mixture of solid and liquid (viscous liquid) phases, while the host medium is considered as a pure elastic medium.

Depending on the depth, temperature and pressure inside the formation, gas hydrates can be either frozen (solid hydrate state) or decomposing if they are outside their stable state zone, for example, when the temperature rises. In the case of frozen gas hydrates, they can be considered as an elastic medium by setting a fluid volume fraction α_1^0 to 0 in Eq. (16)–(19). When gas hydrate melt, the porosity of a layer $\phi = \alpha_1^0 = 1 - \alpha_2^0$ increases until the value of pure liquid (gaseous) state $\phi = 1$. Below one can see the results of numerical simulations for the following parameters of porosity inside the gas hydrate layer: $\phi = 0, \phi = 0.2, \phi = 0.5, \phi = 0.7$. The calculations were carried out for the region (500 m $\times$ 500 m) with a horizontal layer on the depth (150 m, 250 m). The wavefield is excited by a source of the type of volumetric expansion $F(x, y, t) = \delta(x_0, y_0) f(t)$ (δ - Dirac's delta function, localizing the source in point (x_0, y_0)) in (18) at a depth of 30 m. The time function is given by Ricker's wavelet $f(t) = (1 - \omega^2(t - t_0)^2/2) exp[-\omega^2(t - t_0)^2/4]$ with frequency $f_0 = 1$ KHz and pulse delay $t_0 = 2/f_0$. The seismogram was recorded along a vertical observation line passing through the source with a vertical interval between receivers 1 m.

The results of numerical calculations are shown in Fig. 2, 3, 4, 5 and 6. Figures 2, 3, 4 and 5 show seismograms of the magnitude of the mixture velocity

vector, recorded along the vertical observation line passing through the source with an interval 1 m between receivers up to time 0.25 s for different porosities. Figure 6 shows wavefield traces superimposed on each other for the magnitude of mixture velocity vector, recorded by the receiver at a depth of 30 m in the time interval 0.06–0.25 s for various values of the porosity: $\phi = 0, \phi = 0.2, \phi = 0.5, \phi = 0.7$.

For the convenience of classifying the emerging types of waves in the figures, we use the following notation. We denote the P-waves by the letter P, and the S-waves by the letter S. We also denote the reflected waves by the subscripts r and the transmitted waves by t.

From a comparison of the traces for different porosity values in the gas hydrate layer, it can be seen that the greater the porosity, the higher the amplitude of the reflected wave from the upper boundary of the gas hydrate layer (PPr, PSr, SSr). The time of arrival of these waves is obviously the same. We observe a completely different picture for waves reflected from the lower boundary of the gas hydrate layer ($PPtPrPt, PPtSrPt$). For these waves, strong dispersion is observed, which occurs due to the passage of the wave through the porous layer. With an increase in porosity, the velocity increases proportionally, while the amplitude of the waves does not change significantly for the P-wave reflected from the lower layer. For the S-wave reflected from the lower layer, a noticeable increase in amplitude is observed with increasing porosity.

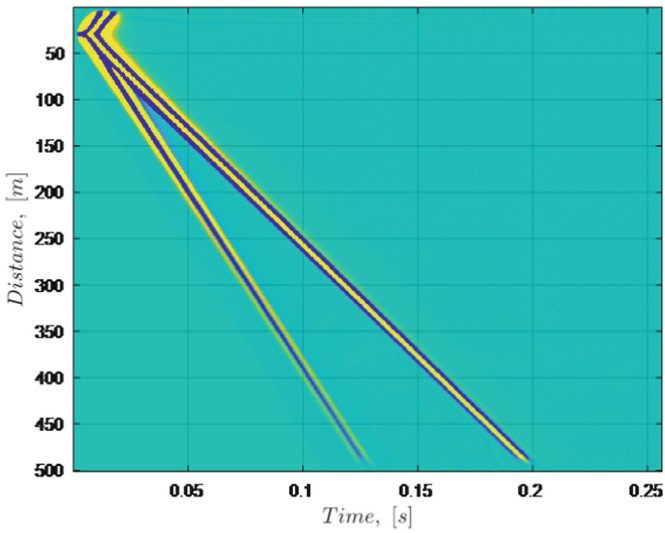

Fig. 2. Seismograms of the magnitude of the mixture velocity vector, recorded along the vertical observation line passing through the source with an interval 1 m between receivers up to time 0.25 s for porosity $\phi = 0$.

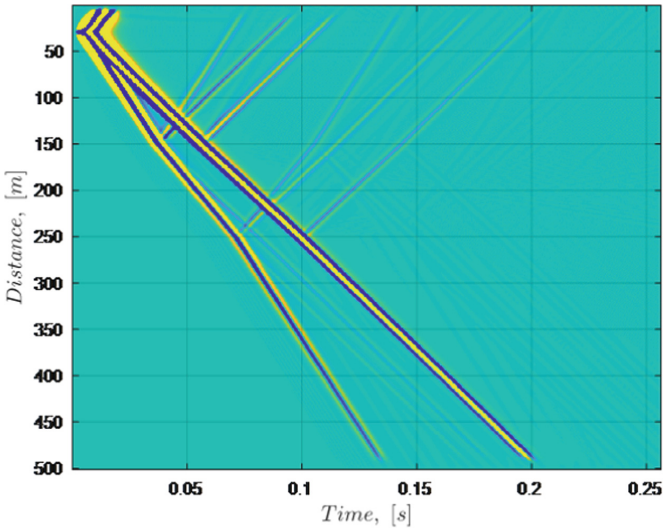

Fig. 3. Seismograms of the magnitude of the mixture velocity vector, recorded along the vertical observation line passing through the source with an interval 1 m between receivers up to time 0.25 s for porosity $\phi = 0.2$.

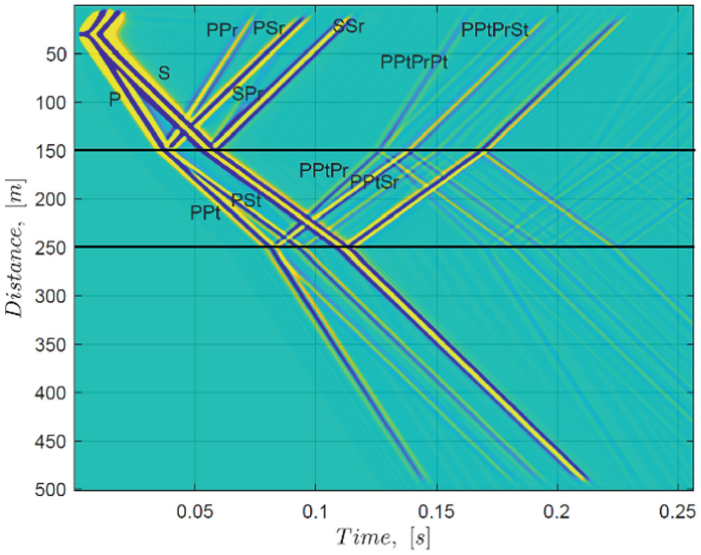

Fig. 4. Seismograms of the magnitude of the mixture velocity vector, recorded along the vertical observation line passing through the source with an interval 1 m between receivers up to time 0.25 s for porosity $\phi = 0.5$.

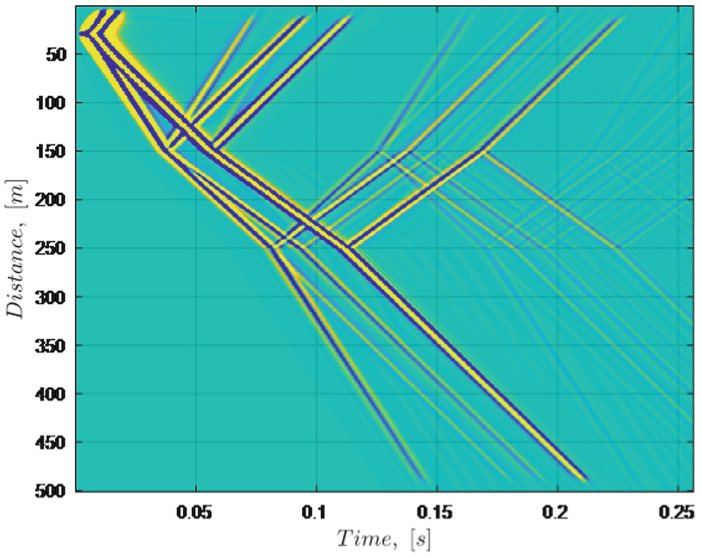

Fig. 5. Seismograms of the magnitude of the mixture velocity vector, recorded along the vertical observation line passing through the source with an interval 1 m between receivers up to time 0.25 s for porosity $\phi = 0.7$.

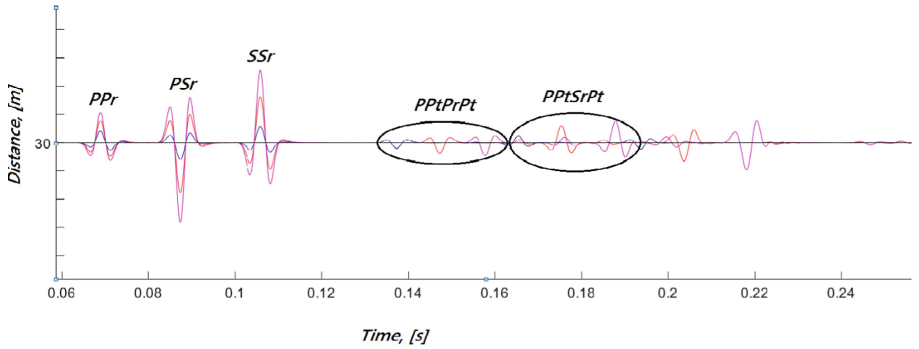

Fig. 6. Traces for the magnitude of the mixture velocity vector recorded by the receiver at a depth of 30 m in the time interval 0.06–0.25 s: black - $\phi = 0$, blue - $\phi = 0.2$, red - $\phi = 0.5$, magenta - $\phi = 0.7$. (Color figure online)

5 Conclusions

A Symmetric Hyperbolic Thermodynamically Compatible (SHTC) model of saturated porous medium is applied to the study of wave propagation in a medium contained a porous layer. The general SHTC model for the case of finite deformation of saturated porous medium is formulated and its linearization for the

modeling of small amplitude waves is presented. The efficient finite difference method on staggered grid is developed and applied to solving a two-dimensional test problems. The features of wave propagation with a change in porosity, which may be a consequence of a change in temperature, are studied. It is numerically shown that for waves reflected from the upper boundary of the porous layer, amplitude variations are observed with a change in porosity, and for waves reflected from the lower boundary of the layer, a strong dispersion is observed depending on porosity. These features of wavefields can be used as the basis for the development of methods for monitoring the evolution of natural accumulations of gas hydrates or permafrost thawing. Further research will include studying the effect of interfacial friction and shear stress relaxation time, which change with temperature, on the behavior of wavefields.

References

1. Romenski, E., Reshetova, G., Peshkov, I., Dumbser, M.: Modeling wavefields in saturated elastic porous media based on thermodynamically compatible system theory for two-phase solid-fluid mixtures. Comput. Fluids **206**, 104587 (2020)
2. Reshetova, G., Romenski, E.: Diffuse interface approach to modeling wavefields in a saturated porous medium. Appl. Math. Comput. **398**, 125978 (2021)
3. Romenski, E., Reshetova, G., Peshkov, I.: Computational model for compressible two-phase flow in deformed porous medium. In: Gervasi, O., et al. (eds.) ICCSA 2021. LNCS, vol. 12949, pp. 224–236. Springer, Cham (2021). https://doi.org/10.1007/978-3-030-86653-2_16
4. Romenski, E., Reshetova, G., Peshkov, I.: Two-phase hyperbolic model for porous media saturated with a viscous fluid and its application to wavefield simulation. Appl. Math. Model. **106**, 567–600 (2022)
5. Biot, M. A.: Theory of propagation of elastic waves in fluid-saturated porous solid. I. Low-frequency range. J. Acoust. Soc. Am. **28**(2), 168–178 (1956)
6. Biot, M. A.: Theory of propagation of elastic waves in a fluid-saturated porous solid. II. Higher frequency range. J. Acoust. Soc. Am. **28**(2), 179–191 (1956)
7. Carcione, J.M., Morency, C., Santos, V.: Computational poroelasticity - a review. Geophysics **75**(5), 75A229–75A243 (2010)
8. Godunov, S.K., Romenskii, E.I.: Elements of Continuum Mechanics and Conservation Laws. Springer, New York (2003). https://doi.org/10.1007/978-1-4757-5117-8
9. Romenski, E.: Hyperbolic systems of thermodynamically compatible conservation laws in continuum mechanics. Math. Comput. Model. **28**, 115–130 (1998)
10. Peshkov, I., Pavelka, M., Romenski, E., Grmela, M.: Continuum mechanics and thermodynamics in the Hamilton and the Godunov-type formulations. Continuum Mech. Thermodyn. **30**, 1343–1378 (2018)
11. Virieux, J.: P-SV wave propagation in heterogeneous media: velocity-stress finite-difference method. Geophysics **51**(1), 889–901 (1986)
12. Graves, R.W.: Simulating seismic wave propagation in 3D elastic media using staggered-grid finite differences. Bull. Seismol. Soc. Am. **86**(4), 1091–1106 (1996)
13. Samarskii, A.A.: The Theory of Difference Schemes. CRC Press, Boca Raton (2001)

14. Moczo, P., Kristek, J., Vavrycuk, V., Archuleta, R.J., Halada, L.: 3d heterogeneous staggered-grid finite-difference modeling of seismic motion with volume harmonic and arithmetic averaging of elastic moduli and densities. Bull. Seismol. Soc. Am. **92**(8), 3042–3066 (2002)
15. Fokin, M.I., Dugarov, G.A., Duchkov, A.A.: Experimental acoustic measurements on sandy unconsolidated samples containing methane hydrate, vol. 4, p. 1940501 (2019). (in Russian)